The Cosmic Ray Energy Spectrum above 3×10^{18} eV Measured by the Akeno Giant Air Shower Array

S. Yoshida[1,2,10], N. Hayashida[1], K. Honda[3], M. Honda[1], S. Imaizumi[4], N. Inoue[4], K. Kadota[2], F. Kakimoto[2], K. Kamata[5], S. Kawaguchi[6], N. Kawasumi[3], Y. Matsubara[7], K. Murakami[8], M. Nagano[1], H. Ohoka[1], M. Teshima[1], I. Tsushima[3], and H. Yoshii[9]

(Submitted to Astroparticle Physics)

[1] *Institute for Cosmic Ray Research, University of Tokyo, Tokyo 188, Japan*
[2] *Department of Physics, Tokyo Institute of Technology, Tokyo 152, Japan*
[3] *Faculty of Education, Yamanashi University, Kofu 400, Japan*
[4] *Department of Physics, Saitama University, Urawa 338, Japan*
[5] *Nishina Memorial Foundation, Tokyo 188, Japan*
[6] *Faculty of General Education, Hirosaki University, Hirosaki 036, Japan*
[7] *Solar-Terrestrial Environment Laboratory, Nagoya University, Nagoya 464-01, Japan*
[8] *Nagoya University of Foreign Studies, Aichi 470-01, Japan*
[9] *Faculty of General Education, Ehime University, Matsuyama 790, Japan*
[10] *Present address: High Energy Astrophysics Institute, Department of Physics, University of Utah, Salt Lake City, UT84112, USA*

ABSTRACT

We report a first result on the cosmic ray energy spectrum above 3×10^{18} eV measured by the Akeno Giant Air Shower Array (AGASA) from July 1990 to February 1994. The analysis method and the energy resolution of the AGASA experiment are described in some detail. The flattening of the spectrum around 10^{19}eV (ankle) is observed with a significance of 2.9σ. If we express the differential energy spectrum of cosmic rays of energy E (in eV) with an ankle energy E_a as $J(E) = \kappa(E/E_a)^{-\gamma} m^{-2}\,\mathrm{sec}^{-1}\,sr^{-1}\mathrm{eV}^{-1}$, γ for $10^{18.5}\mathrm{eV} \leq E \leq E_a$ is in good agreement with that from the previous experiment and is 3.2±0.1. The slope γ above E_a depends strongly on the value E_a. For the case E_a=10^{19}eV, $\kappa = (2.3^{+0.1}_{-0.2}) \times 10^{-33}$ and γ=$2.3^{+0.5}_{-0.3}$ for $10^{19}\mathrm{eV} \leq E \leq 10^{20}\mathrm{eV}$. If E_a=$10^{18.8}$eV, then $\kappa = (1.0 \pm 0.1) \times 10^{-32}$ and γ=$2.7^{+0.2}_{-0.4}$ for $10^{18.8}\mathrm{eV} \leq E \leq 10^{20}\mathrm{eV}$, after correcting for both the statistical error and the energy resolution of the present experiment. If we interpret the present results assuming an extragalactic origin for cosmic rays above 10^{19} eV, the observed data is consistent with either a homogeneous and isotropic distribution of sources or with localized sources at redshift of greater than $\sim$ 0.1. A (1.7∼2.6)×10^{20}eV event was observed on December 3, 1993 from the direction of l=131° and b=-41°. This shower energy is a factor 3 larger than the second highest energy event.

1.INTRODUCTION

The origin of the most energetic cosmic rays extending over 10^{20} eV is of great astrophysical interest. If these are of extragalactic origin, modifications in the energy spectrum as a result of the interaction between the cosmic ray nucleons or nuclei and the 2.7 K black body photons should yield important information about their origin [1-6]. In spite of considerable efforts for more than 30 years on spectrum measurements at Volcano Ranch [7], at Haverah Park [8], at Sydney [12], at Yakutsk [13], at Dugway [9] and at Akeno [10], conclusive answers have not yet been obtained, the results being limited by statistical and systematic errors and the energy resolutions of the experiments.

In order to study the highest energy cosmic rays, we constructed a very large surface array covering an area of about 100 km^2 area, called the Akeno Giant Air Shower Array (AGASA), about 130km west of Tokyo. 95 percent of the surface detectors have been operated since the spring of March 1991 and full operation started on April 1993. The aperture for collecting the highest energy cosmic rays is the largest in the world at present and event statistics are expected to be significantly improved in the near future. In this paper, we describe the analysis method of the AGASA experiment in some detail and a first result on the energy spectrum of cosmic rays with energies beyond 3×10^{18} eV measured by the AGASA from July 1990 to February 1994. In this analysis, events of good quality are selected by requiring that they hit well inside the array boundary with zenith angles less than 45°.

In Section 2, we briefly describe the experimental apparatus of the AGASA. The details of the array have been described in our earlier paper [11]. Shower analysis procedures and resultant energy resolutions are also presented. In Section 3, we present the observational results on the energy spectrum. The spectral slope of the primary cosmic ray spectrum is estimated using Monte Carlo simulations which take into account the energy resolution. Some discussion of our results is presented in Section 4. We compare our data with those of other experiments and discuss the significance of the spectrum structures. Assuming the cosmic rays above 10^{19} eV to be extragalactic in origin, we compare our results with calculations on their propagation in intergalactic space by Yoshida and Teshima [6] and examine the implications. The conclusions are summarized in section 5.

2.EXPERIMENTS

In the AGASA, 111 density detectors are arranged with inter-detector separation of about 1 km and they are sequentially connected by a pair

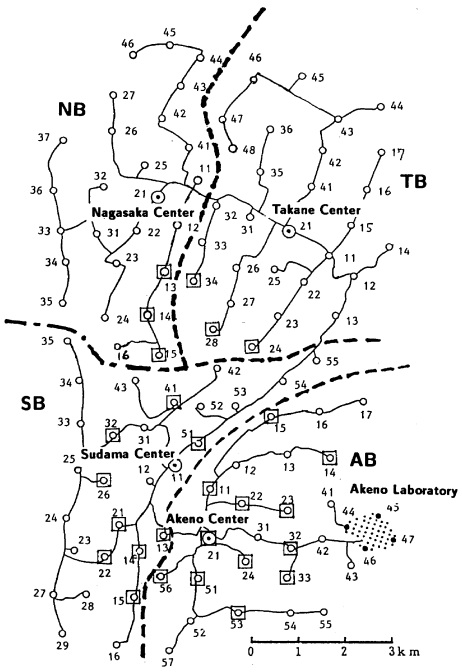

Figure 1: A schematic view of the AGASA. Open circles are scintillation counters and squares are muon detectors. The solid line show the routes of optical fiber cables for data communication network.

of optical fibers. The schematic view of the array is shown in figure 1. Each surface detector consists of plastic scintillators of 2.2 m^2 area, which are viewed by a 125 mm diameter Hamamatsu R1512 photomultiplier tube (PMT). To measure muons associated with giant air showers, shielded proportional counters are deployed at 27 positions of the 111 surface detectors. The absorber shield consists of either a thick iron plate and a thin lead plate or concrete. The threshold energy of muons is about 0.5 GeV. The AGASA is divided into 4 branches, the "Akeno Branch (AB)", the "Sudama Branch (SB)", the "Takane Branch (TB)", and the "Nagasaka Branch (NB)". A data processing and storing station, called a "Branch Center", is placed at the center of each of the four branches. A new data acquisition system has been developed and installed for the AGASA which makes it possible to control and operate all detectors through a set of commands transmitted from the central computer.

2.1 The Data Acquisition System

The data acquisition system has been developed for processing data to and from all the surface detectors with a flexible response to seasonal changes of temperature, variations of gain in the amplifiers and movement

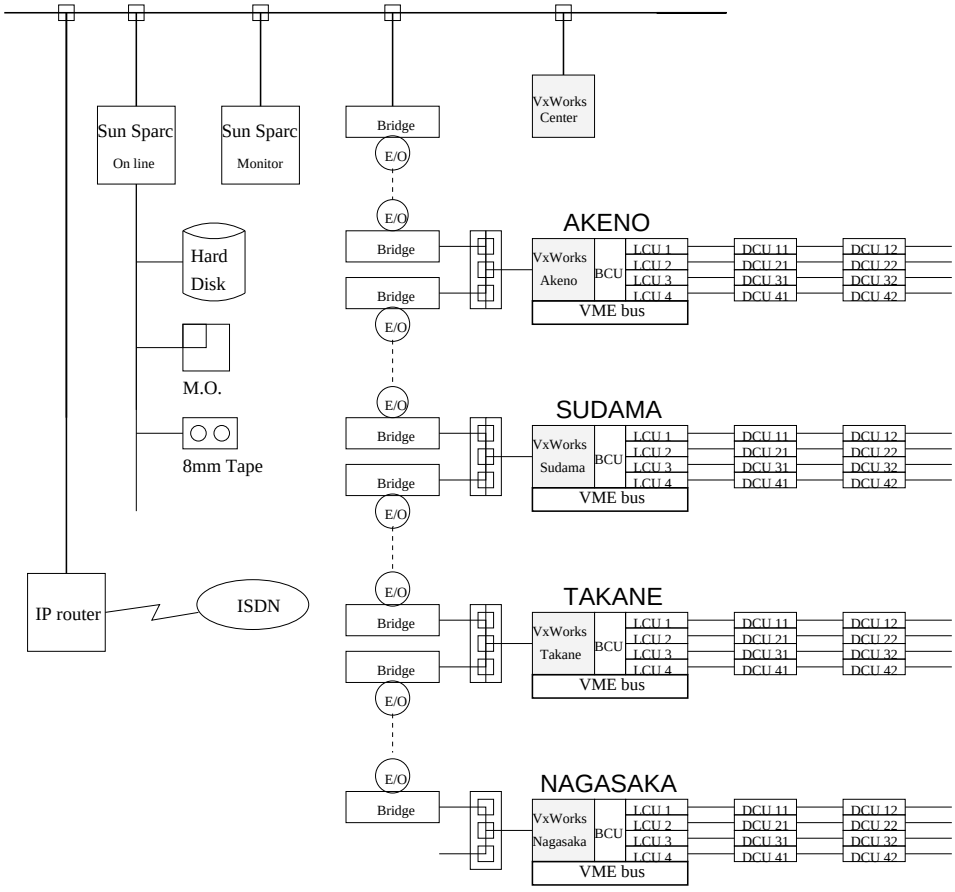

Figure 2: Block diagram of the AGASA data acquisition system.

of detector positions [11]. Figure 2 shows the block diagram of the optical fiber network for the whole system. The system consists of the detector control unit (DCU) for service of each detector, the line control unit (LCU) for managing each string from the branch center and the branch control unit (BCU) which controls all the data flow at the branch center. The BCU is managed by a MOTOROLA 68030 microprocessor running under the VxWorks operating system. The operation procedures are managed and monitored by the Sun SPARC through an optical ethernetwork of 10Mbps.

The operation procedure for a single RUN is the following: First, the BCU in each branch center examines the connection status for all DCUs through the LCU and lists the on-line detectors and sets the high-voltage of each detector. Next, propagation times from each detector to the BCU are measured and delay times from all BCUs are adjusted to be the same for triggering. Then the data acquisition starts. The signals from the amplifier in each detector are recorded immediately in the cyclic memory of each

DCU. At the same time, each DCU sends a signal to the BCU every 3.2 μ sec to inform it whether the detector was hit by particles or not. The BCU judges coincidence conditions with this information from all DCUs.

A trigger is generated whenever more than five fold coincidence occurs among neighboring detectors within a gate width of 25.6 μ sec after adjusting the propagation time in optical fibers and modules from all detectors to be the same. To reduce the accidental coincidences, the trigger judgement is done through a comparison of the pattern of hit-detectors with those stored in the BCU. About 900 expected patterns with combination of five detectors are selected in each branch by the Monte Carlo simulation. When a trigger is generated, each DCU stops data acquisition and searches for the corresponding data in the cyclic memory within 60 μ sec before and after the coincidence time. The LCU then demands the selected data from the DCUs. After the receipt of data from all the DCUs on its string, the data is transferred to the BCU. All the data received in the BCU are stored on the hard disk under the control of the Sun SPARC through the packet communication with the VxWorks operating system. After 1000 events have been collected, the BCU stops the data acquisition and collects the calibration data such as the counting rate of each detector per minute.

The trigger rate in each branch is about 50 events per hour and hence about 200 per hour in total. Each RUN continues for about 20 hours. 90% of all data are background events recorded by accidental coincidence.

2.2 Density Measurements

The anode signal of PMT is shaped to an exponential form with a decay constant of 10 μ sec which is then discriminated to give a square pulse. The width of this pulse is proportional to the logarithm of the number of particles incident over the detector. The resultant dynamic range is $0.2\sim\ 5 \times 10^4$ particles.

The absolute gain is adjusted to make a peak of the pulse width spectrum shown in figure 3 to be 10μ sec. This spectrum is monitored and stored by the data acquisition system in each RUN. The peak channel of the spectrum which relates to a "single particle" is determined in every RUN and is used to calibrate the overall gain. An example of a daily variation of the peak channel of a typical detector is shown in figure 4.

2.3 Method of Primary Energy Estimation

We observe cosmic rays through giant air showers (GAS) initiated by the cosmic ray primaries. The surface detectors sample the local particle densities in the GAS as a function of distance from the shower core. An

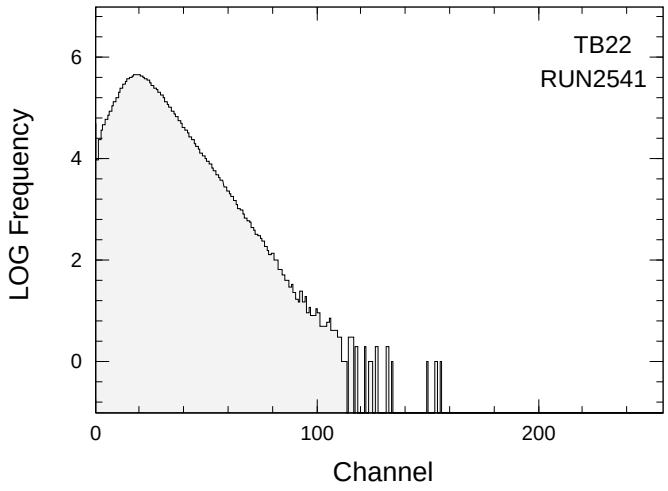

Figure 3: Pulse width spectrum of a typical detector in one run (RUN2541). 1 channel corresponds to 500 n sec. This distribution is continuously monitored during every RUN.

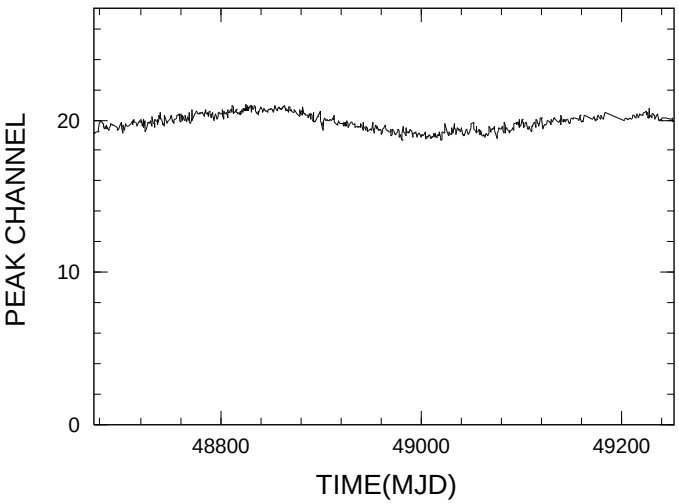

Figure 4: Variations of the peak channel value of the pulse width spectrum of a typical detector as a function of modified Julian days. These variations are used for the calibration of each detector in data analysis.

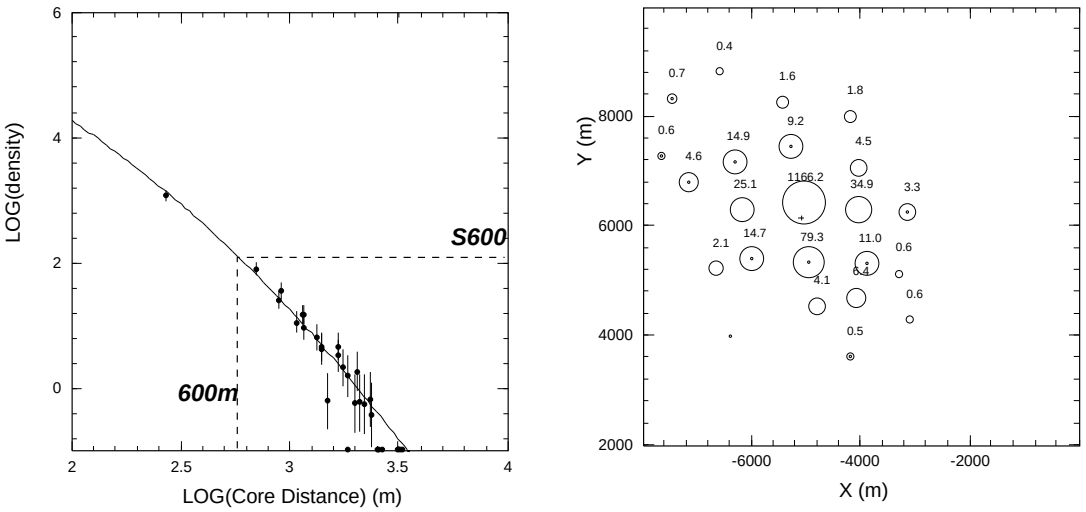

Figure 5: An example of a shower observed by the AGASA. left: Lateral distribution of the charged particles. right: Density map. Radius of each circle corresponds to the logarithm of the particle density m^{-2}.

example of an observed event is shown in figure 5. Hillas et al. showed that local particle density at 600 m from the shower axis (S(600)) is proportional to the primary energy and is a good energy estimator, since this value depends only weakly on the primary mass and fluctuations in cascade development [14]. The conversion relation from S(600) to primary energy at Akeno level is evaluated by Monte Carlo simulation up to 10^{19} eV (Dai *et al.,* 1988 [15]) as

$$E = 2.0 \times 10^{17}\ S_0(600) \quad eV, \tag{1}$$

where $S_0(600)$ is the S(600) for a shower of vertical incidence. Since this value $S_0(600)$ attenuates with zenith angle, we need to correct the observed $S_\theta(600)$ at zenith angle θ to $S_0(600)$ at the vertical by the observed attenuation length. This curve is obtained as (Yoshida *et al.,* 1994 [16]):

$$S_\theta(600) = S_0(600)\exp[-\frac{X_0}{500}(\sec\theta - 1) - \frac{X_0}{594}(\sec\theta - 1)^2], \tag{2}$$

where X_0 is 920 gcm^{-2}, the atmospheric depth at Akeno. We use this relation up to the highest energies in the present analysis.

Therefore, in this experiment it is most important to determine $S_\theta(600)$ from the observed lateral distribution of particle densities.

2.4 Shower Analysis Procedure

Our shower analysis procedure is based on an iterative process to find an arrival direction of a primary cosmic ray and to search for its core position and $S_\theta(600)$.

First, we assume that an initial core is located at the center of gravity in the density distribution of an observed event. Then we search for an arrival direction (zenith θ, azimuth ϕ) to minimize the function,

$$\chi^2 = \frac{\sum_i^n (T_i + z_i'(\theta,\phi)/c - T_d - \tau)^2 / T_{\sigma,i}}{n-3}. \tag{3}$$

Here T_i is the arrival time of particles in the ith detector, z_i' is its z' value in a coordinate system in which the z' axis is along the shower axis (θ,ϕ), c is the speed of light, and τ is a constant value. T_d and T_σ are the delay time of the first particle observed by each detector from the plane shower front and its fluctuation of shower particles around the average. These values were determined in the earlier analysis [17] and decrease with the number of incident particles ρ as

$$T_d = 2.6(1+\frac{R}{30})^{1.5}\rho^{-0.5} \qquad n \text{ sec} \tag{4}$$

$$T_\sigma = 2.6(1+\frac{R}{30})^{1.5}\rho^{-0.3} \qquad n \text{ sec} \tag{5}$$

where R is the distance in m from the shower axis. The whole sky is divided into grids with a spacing of 0.2° and we search for the grid point to minimize χ^2 value given by Eq.(3). Then all the detector locations are transformed to those on a plane normal to the determined arrival direction. Observed particle densities are fitted to an empirical formula for the lateral distribution function (referred to as LDF hereafter) to search for the location of the shower core in the plane. The LDF used in the present analysis is given by:

$$\rho(R) = C(\frac{R}{R_M})^{-1.2}(1+\frac{R}{R_M})^{-(\eta-1.2)}(1.0+(\frac{R}{1000})^2)^{-0.6}, \tag{6}$$

$$\eta = 3.97 - 1.79(\sec\theta - 1).$$

Here R_M is the Moliére unit (91.6 m at Akeno), calculated at two radiation lengths above the central laboratory at the Akeno Observatory. C is a normalization factor and η is a parameter which determines the slope of the LDF at $R > R_M$ [16]. In the fitting procedure, we search for the core location and a factor C to maximize the likelihood function represented as

$$\mathrm{L}(\rho_{LDF}) = \prod_i^n \mathrm{L}_0(\rho_{LDF}, \rho_{obs,i}), \tag{7}$$

$$\mathrm{L}_0(\rho_{LDF}, \rho_{obs,i}) = \frac{1}{2\pi\sigma_\rho} \exp[-\frac{1}{2}\frac{(\rho_{obs,i} - \rho_{LDF})^2}{\sigma_\rho^2}],$$

where $\rho_{obs,i}$ is the observed particle density in the ith detector and ρ_{LDF} is the particle density predicted from the LDF. σ_ρ is the fluctuation of particle densities due to statistics, resolution of the detector, and uncertainty in the core position determination. This σ_ρ was determined by the previous analysis [18]. These processes to search for the arrival direction and the core location are repeated 4 times to give the most probable values. Then the particle density at 600 m from the core, $\mathrm{S}_\theta(600)$, is calculated using the best estimated core position and the LDF. The estimated $\mathrm{S}_\theta(600)$ is transformed to the equivalent value in the vertical direction, $\mathrm{S}_0(600)$, using the attenuation curve expressed by Eq.(2). Finally $\mathrm{S}_0(600)$ is converted to an energy for the primary cosmic ray using Eq.(1).

2.5 Energy Resolution and Systematic Errors

We discuss the AGASA energy resolution and systematic errors before presenting the observed energy spectrum. The energy resolution corresponds to S(600) resolution in our experiment. The accuracy of the S(600) estimation depends on fluctuations in the shower cascade development in the atmosphere, the resolution of the scintillation detector, statistical fluctuation of observed particles at each surface detector. Fluctuations of S(600) due to the cascade development have been studied in detail by the Monte Carlo method [15]. It depends on the shower zenith angle, $\sim$ 15% for vertical showers and $\sim$ 40% at $\theta = 45°$ for EAS of energies of 10^{18} eV. The FWHM (full width at half maximum) of the scintillation detector is $\sim$ 80% for a vertically incident particle on the scintillator [18]. This means our detector resolution is $\sim$ 25% in case of 10 particles passing over the detector.

We simulated artificial showers taking these fluctuations into account in order to derive the AGASA energy resolution. The events simulated were analyzed by the same procedure described in the previous subsection and comparison between input energies and analyzed ones gives the resolution of our S(600) estimation. Figure 6 shows the fluctuation of the S(600) determination obtained from the Monte Carlo simulation for four S(600) input values. In figure 7 is presented the energy dependence of these S(600) resolutions. One can see that the larger the zenith angle, the poorer the resolution becomes, because of the increasing importance of fluctuations in cascade development and the decreasing effective scintillator size. The S(600) is determined within an accuracy of about $\pm$30% for events with $E \geq 10^{19}$ eV and $\sec\theta \leq 1.4$.

Energy uncertainty arises also from systematic errors in the calibration

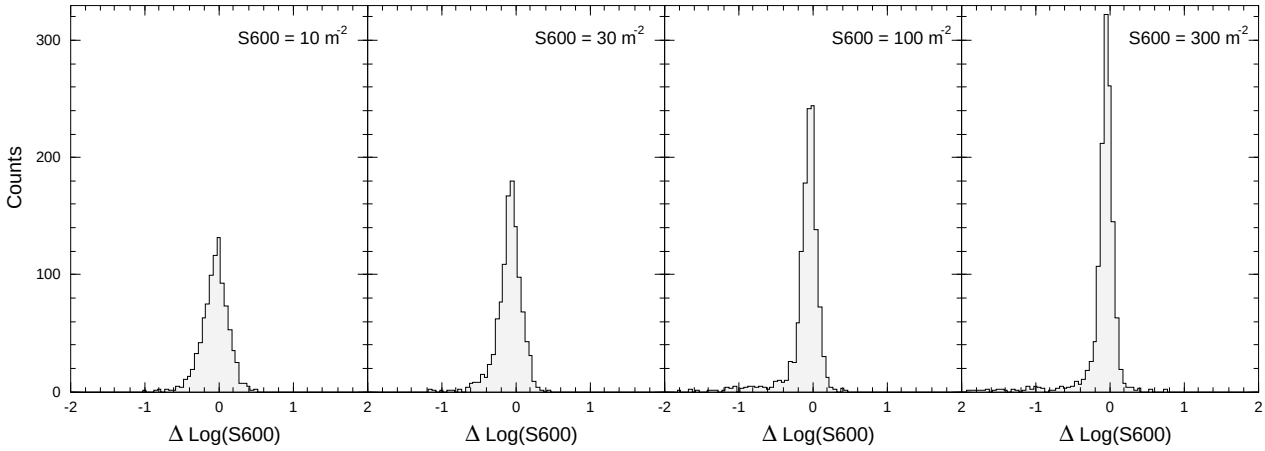

Figure 6: The fluctuation of S(600) determination for showers of $\sec\theta \leq 1.2$. Horizontal axis shows the logarithm of the ratio of the output and input S(600). The widths of these distributions correspond to the energy resolution.

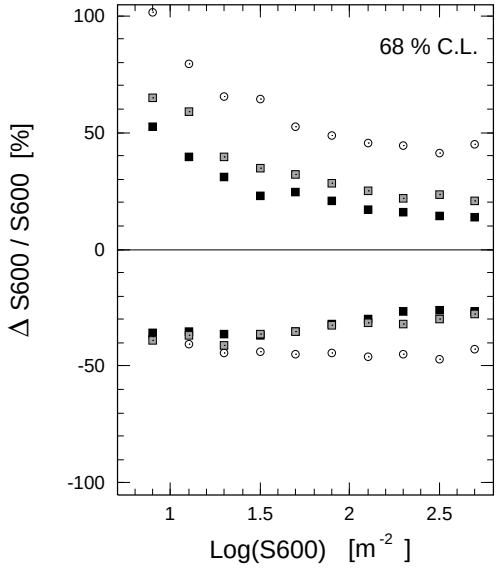

Figure 7: S(600) dependence of S(600) resolution. Upper and lower limits are shown which encompass 68% of the data. Closed squares correspond to the events with $1.0 \leq \sec\theta \leq 1.2$, shaded squares to the events with $1.2 \leq \sec\theta \leq 1.4$, and open circles to the events with $1.4 \leq \sec\theta \leq 1.6$. S(600) of 10 m^{-2} corresponds to 2×10^{18} eV for vertical showers.

of each detector, uncertainties in the shape of the LDF, uncertainties in the attenuation curve of S(600), and energy conversion from the S(600) parameter.

Uncertainty in the calibration of each detector is mainly caused by the daily variance of gain and decay constant of the exponential pulse. The gain has been determined within an accuracy of ~ 50 n sec in every RUN by monitoring the pulse width spectrum as shown in figure 4. Since the decay constant of the pulse is 10μ sec, systematic error due to the gain uncertainty is about $\pm 0.5\%$. The decay constant in the exponential pulse shape also changes due to seasonal changes of temperature. We estimated the variance of the decay constant from changes in the slope of the pulse width spectrum to conclude that the seasonal variance is within 1%. This could cause systematic errors of 2% for 10 particles and 5% for 100 particles per detector.

The probable systematic errors due to limited accuracy in the determination of η in the LDF have been discussed in our recent paper [16]. We fitted the observed GAS events to the LDF with η varying within its determination errors to find that the systematic deviation in S(600) due to the uncertainty in the LDF is $\sim \pm 5\%$ for near vertical showers, $\sim \pm 10\%$ for showers with $\sec\theta = 1.4$, and $\sim \pm 20\%$ for showers with $\sec\theta = 1.6$. In the same paper, systematic errors due to the attenuation curve of S(600) have been also discussed. The limited accuracy of the attenuation curve represented by Eq.(2) causes uncertainty in the estimated value of $S_0(600)$ after conversion from $S_\theta(600)$. The probable systematic uncertainty in energy estimation due to both the uncertainty in the LDF and the attenuation curve have been estimated to be no more than $\pm 10\%$ (for $\sec\theta = 1.1$) and $\pm 20\%$ (for $\sec\theta = 1.4$), even if both the systematic errors shift the estimated energy in the same direction.

According to the simulation by Dai et al.[15], the uncertainties in the energy conversion relation given by Eq.(1) described before is irrespective of the primary composition and interaction models. The systematic error rather depends on the lateral distribution of electrons (LDE) used in the simulation, where the analytical LDE function is applied to each electron after its generation in the shower development. Details of the LDE and the value for the radiation length at the observation level are differ in various calculations. In Dai et al. the lateral distribution function was chosen by comparing simulation results with the experiment around 10^{17}eV up to 1000m from the core. Since electromagnetic cascades may be scalable to the highest energy, systematic errors in the energy conversion relation given by Eq.(1) may not be significant. The Yakutsk group is trying to deter-

mine the S(600) to energy conversion relation experimentally [13]. They are measuring energies carried by electromagnetic components and muons (neutrinos), not only on the surface and underground, but also in the atmosphere through Ćerenkov light emission measurements. The conversion relation determined from the Yakutsk experiment is 15% larger than our relation based on simulations.

3.RESULTS

In this section are presented our observational results on the energy spectrum of cosmic rays. In order to determine the primary spectrum with as much precision as possible, some cuts on the data have been introduced. First we discuss the criteria for selection of the observed showers and the collecting area of our array. Then the observed energy spectrum is presented. The spectral shape and absolute flux of the cosmic ray primaries are estimated from the observed spectrum using the maximum likelihood method with Monte Carlo simulation, taking into account the AGASA energy resolution described in the previous section.

3.1 The Shower Selection and Collecting area

In order to measure the spectral shape as precisely as possible, we have used only those showers which have density information from more than 6 detectors, whose cores are located well within the boundary of each branch of the array, and whose zenith angles satisfy $\sec\theta \leq 1.4$, because inclined showers are reconstructed with poorer resolution and larger systematic errors as described in the previous section. Then we set the discrimination at a certain value of the likelihood function in the density fitting represented by Eq.(7) to cut the poorly fitted data. All these procedures result in energy resolution better than $^{+65\%}_{-40\%}$ for $E \geq 3 \times 10^{18}$ eV and $^{+28\%}_{-32\%}$ for $E \geq 2 \times 10^{19}$ eV. Finally we excluded all showers recorded in RUNs where operating conditions were not stable due to the failure of network communication or other causes.

To estimate the collecting area of each branch in the present experiment, a large number of artificial showers were simulated over a larger area than the branch area with directions sampled from an isotropic distribution. These were analyzed by the shower analysis procedure using the criteria described above. By multiplying the resultant collecting area and the observation time of each branch (Akeno Branch 885.0429 days, Sudama Branch 1036.7774 days, Takane Branch 1089.0915 days and Nagasaka Branch 792.6672 days), the total exposure for the present analysis is shown in figure 8. The exposure is constant in the region above 10^{19} eV while it depends strongly on the

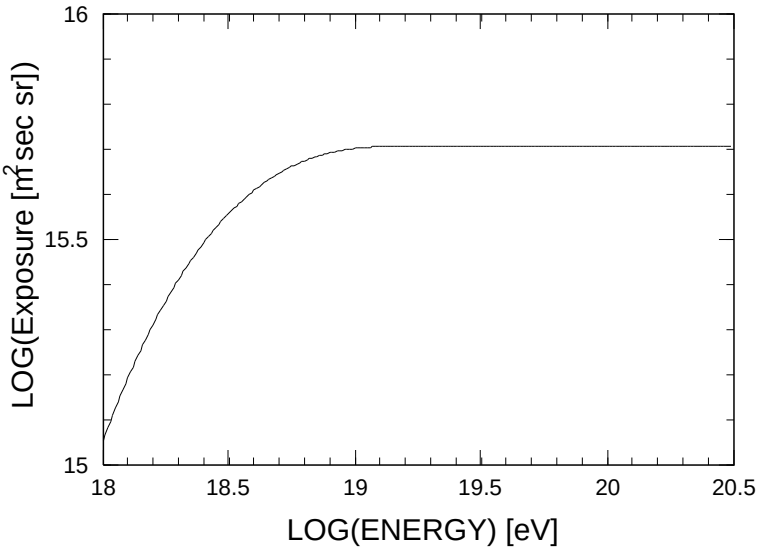

Figure 8: The exposure of the AGASA for the present analysis.

primary energy in the lower energy region, which causes larger systematic errors in deriving the spectrum. In this report we present the spectrum only above 3×10^{18} eV to avoid this difficulty.

3.2 Observed Energy Spectrum

The energy spectrum observed by the AGASA is presented by closed circles in figure 9, multiplied by E^3 in order to emphasize details of the steeply falling spectrum. The error bars represent the Poissonian upper and lower limits at 84%. It is seen that there is a change of slope in the spectrum around 10^{19} eV (ankle). The AGASA spectral slope below this energy is consistent with that obtained from the 1 km^2 array, which has less systematic error than the AGASA in determining the slope because of the uniform detection efficiency between 10^{17} eV and 10^{19} eV [10]. The significance of the ankle will be discussed in the next subsection.

The most energetic event measured by the AGASA was detected on December 3, 1993. The estimated energy is $(1.7 \sim 2.6) \times 10^{20}$eV. The energy of the next largest one is 6.7×10^{19}eV, and there are no events between them. 90%C.L. upper limits are shown by arrows in the figure. Details of the largest event will be described in 3.4.

3.3 The Most Probable Primary Energy Spectrum

The spectrum presented in figure 9 has been derived from a limited number of events with limited accuracy in energy determination. It is nec-

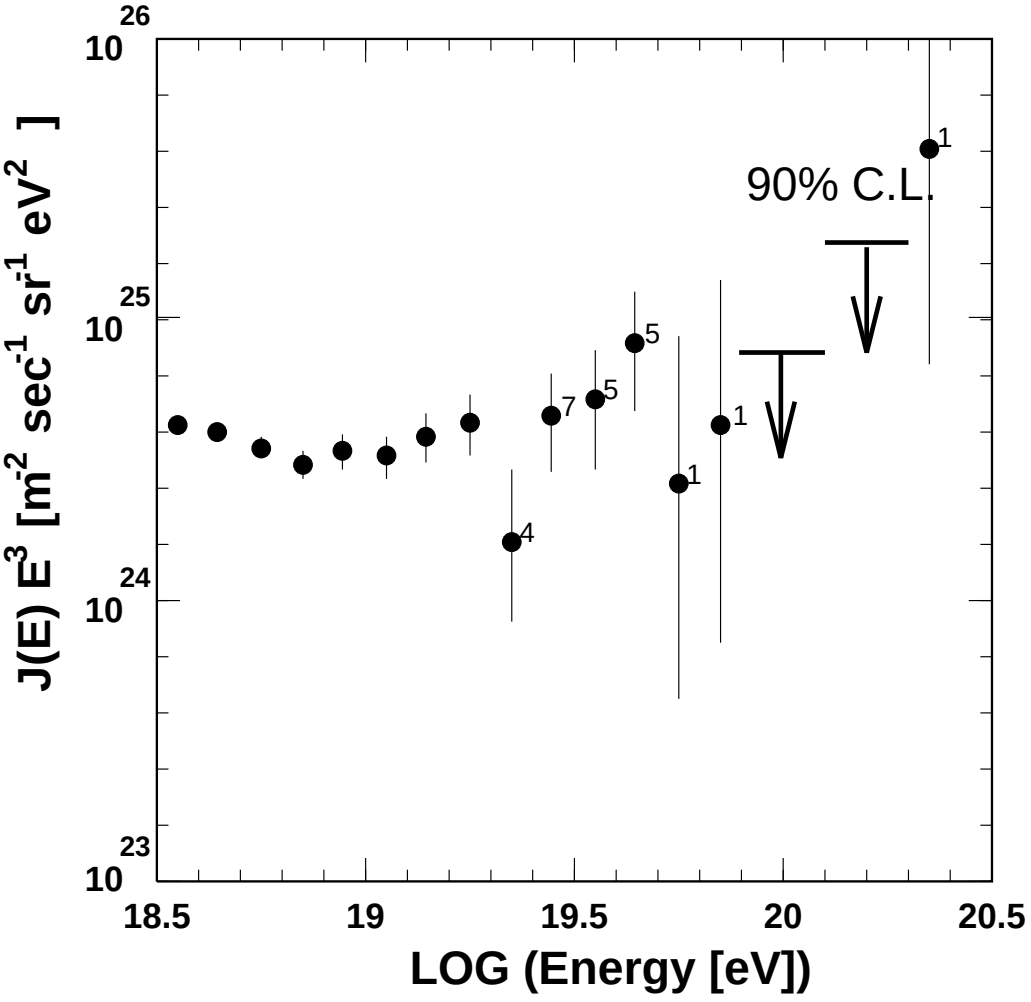

Figure 9: The energy spectrum determined by the present experiment. Numbers attached to the closed circles show the number of events in each bin.

essary to take into account both the statistical error and the determination error in order to derive the real primary spectrum from the observed one. We use a Monte Carlo method to sample the number of events expected in each energy bin for a given primary energy spectrum and compare with the observed data. The procedures of this simulation, which we call the "spectrum Monte Carlo" hereafter, are described in the Appendix.

For an expected number of events in the ith energy bin, μ_i, the probability of observed events ($N_{obs,i}$) in that bin is assumed be the Poisson probability $P(\mu_i, N_{obs,i})$. The likelihood function for the evaluation of the spectrum is given by

$$\mathrm{L} = \prod_i P(\mu_i, N_{obs,i}). \tag{8}$$

The most probable primary spectrum is obtained by the values μ_i which maximize L. The μ_i values are too small in the present case for the Gaussian approximation to apply. Therefore the distribution of L values does not follow the χ^2 distribution. In order to determine the distribution of L, $G(\mathrm{L})$, for a given spectrum, L is evaluated by the Monte Carlo simulation by sampling the number of events in ith energy bin from the Poisson distribution of mean value μ_i. From many trials of this procedure, $G(\mathrm{L})$ is determined for a given energy spectrum. Then the likelihood significance of L, $C(\mathrm{L})$, for the observed number of events, $N_{obs,i}$ and the expected number of events, μ_i is evaluated as the summation of $G(\mathrm{L}')$ values for $\mathrm{L}' < \mathrm{L}$ as

$$C(\mathrm{L}) = \int_0^{\mathrm{L}} G(\mathrm{L}')d\mathrm{L}'. \tag{9}$$

First, we examine whether the observed spectrum can be represented by a single power law spectrum. From the measurements by the Akeno $1km^2$ array, we have determined the spectral slope above $10^{17.8}$ eV to be 3.2 ± 0.1 [10]. This result is consistent with the present AGASA results in the region below 10^{19} eV. In the overall energy region including energies above 10^{19} eV, the likelihood significance of the single power law spectrum $E^{-3.2}$ is evaluated by Eq.(9) and is 1.75×10^{-2}. The expected number of events above $10^{18.5}$ eV in each bin are listed in Table 1, together with the observed ones. The total number of events above 10^{19} eV estimated by the spectrum Monte Carlo is 72.3, while 97 events have been observed. Hence the significance of the flattening above 10^{19} eV, or an ankle around 10^{19} eV, is 2.9 σ.

Next, we examine the primary energy spectrum with a combination of

Table 1: Number of Events Observed and Expected from three different energy spectra

Energy Bin Log(E [eV])	Observed	Expected from $\sim E^{-3.2}$	Expected from Eq.(11)	Expected from Eq.(11')
18.55	312	319.34	310.03	314.15
18.65	206	211.18	205.54	206.20
18.75	124	131.53	129.30	129.61
18.85	72	81.75	79.06	80.48
18.95	52	47.52	47.79	50.36
19.05	32	28.88	29.85	32.99
19.15	24	17.63	19.85	21.17
19.25	17	10.61	14.88	16.00
19.35	4	6.18	11.03	10.35
19.45	7	3.62	7.94	6.62
19.55	5	2.05	5.35	4.47
19.65	5	1.43	4.37	2.93
19.75	1	0.80	2.79	2.02
19.85	1	0.45	2.26	1.53
$\geq$19.90	1	0.60	6.97	3.18

two different power indexes below and above the ankle energy E_a as

$$\frac{dJ}{dE} = \begin{cases} \kappa(\frac{E}{E_a})^{-\gamma_0} & 10^{18.5} eV \leq E \leq E_a \\ \kappa(\frac{E}{E_a})^{-\gamma_1} & E_a \leq E \end{cases} \tag{10}$$

The slope in the lower energy region, γ_0, is fixed to 3.2 which has been determined by the Akeno $1km^2$ array. We search for the most probable values for κ, E_a, γ_1 using the spectrum Monte Carlo and the likelihood test given by Eqs.(8) and (9) with data points below 10^{20}eV.

The slope γ_1 depends on E_a and the results are listed in Table 2. The likelihood significance for each trial spectrum below $10^{19.9}$ eV is also listed in Table 2. This value is calculated using Eq.(9) and a larger value means better matching between the trial spectrum and the data. Though the likelihood significance is largest for $E_a = 10^{19}$eV, the differences among the E_a's are not large enough for confident discrimination.

The probable primary spectrum for E_a=10^{19}eV is represented by

$$\frac{dJ}{dE} = (2.3^{+0.1}_{-0.2}) \times 10^{-33} (\frac{E}{10^{19}})^{-\gamma_1} \quad m^{-2} sec^{-1} sr^{-1} eV^{-1} \tag{11}$$

where γ_1=$2.3^{+0.5}_{-0.3}$ for $10^{19} \leq E \leq 10^{20}$eV. For E_a=$10^{18.8}$eV, it is

$$\frac{dJ}{dE} = (1.0 \pm 0.1) \times 10^{-32} (\frac{E}{10^{18.8}})^{-\gamma_1} \quad m^{-2} sec^{-1} sr^{-1} eV^{-1} \tag{11'}$$

Table 2: Best fitted slope between ankle energy and $10^{19.9}$eV are listed with the likelihood significance obtained by Eq.(9). Errors of the slope are at 68 % confidence level evaluated by Eq.(9). Expected number of events above $10^{19.9}$ eV estimated from the extrapolation of the spectra with different power indices are also listed.

Ankle Energy Log(E_a)eV	Slope γ_1 between E_a and $10^{19.9}$eV	Likelihood Significance $\leq 10^{19.9}$eV	Expected Number of Events $\geq 10^{19.9}$eV	Probability of Cutoff $\geq 10^{19.9}$eV
19.1	$2.1^{+0.7}_{-0.3}$	0.829	9.20	1.0×10^{-3}
19.0	$2.3^{+0.5}_{-0.3}$	0.929	6.97	7.5×10^{-3}
18.9	$2.4^{+0.5}_{-0.2}$	0.912	6.05	1.7×10^{-2}
18.8	$2.7^{+0.2}_{-0.4}$	0.897	3.18	1.7×10^{-1}

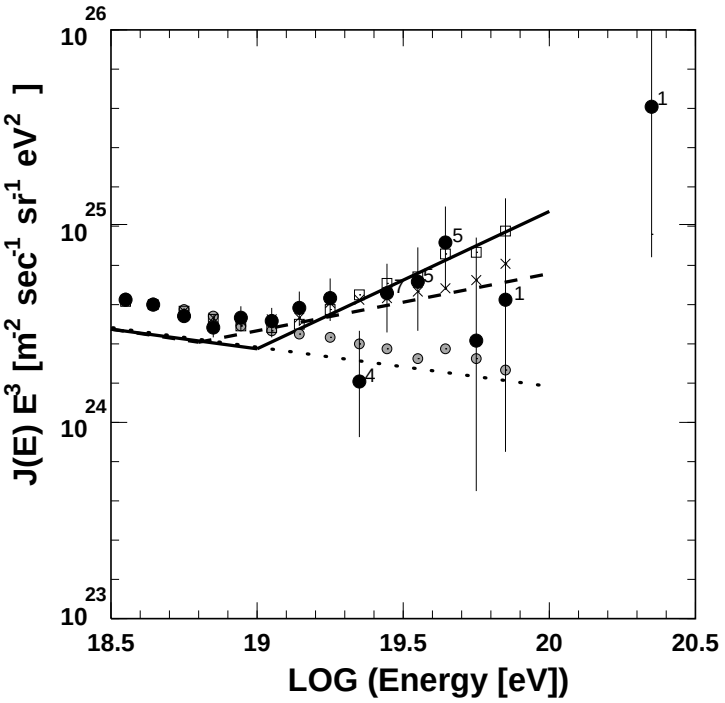

Figure 10: Derived primary energy spectra expressed by Eqs.(11)(a solid line) and (11')(a dashed line) and the expected values in each bin simulated under the assumptions of these spectra with the energy resolution of the present experiment (open squares and crosses). Black dots with error bars are the law data(see figure 9). The case of a single power upto the highest energy is also shown by a dotted line and shaded circles.

Table 3: Various parameters of the most energetic event.

Event Number	#akn25400-0296	
Date	December 3, 1993	
Incident Time	12:32:47	UT
Zenith Angle	22.9	degrees
Error circle in arrival direction determination	1.0°	radius
Determined S(600)	892∼1065	m^{-2}
Primary Energy	(1.7∼2.6)× 10^{20}	eV
Right Ascension	18.9	degrees
Declination	21.1	degrees
Galactic Longitude	131	degrees
Galactic Latitude	-41	degrees

where γ_1=$2.7^{+0.2}_{-0.4}$ for $10^{18.8} \leq E \leq 10^{20}$eV.

Listed in Table 1 are the number of events observed and expected from both Eq.(11) and Eq.(11′). For these two cases, the most probable primary spectrum and expected values in each bin under the energy resolution of the present experiment are compared with experimental results in figure 10. In the same figure, the case of a single slope 3.2 up to the highest energy is also compared. Solid, dashed and dotted lines are input spectra, and open squares, crosses and shaded circles are corresponding simulated values from the spectrum Monte Carlo. Energy determination errors cause the observed fluxes to exceed the true fluxes.

The expected number of events in the highest energy region depends strongly on the assumed slope of the spectrum above the ankle. In Table 2 are listed the number of events above $10^{19.9}$ eV expected from extrapolating the primary energy spectra with different power indexes. Also listed for each case is the Poisson probability for observing no more than 1 event above this energy.

3.4 The Highest Energy Event

The highest energy event in the data set described in subsection 3.1 is shown in Fig.11. The parameters of this event are listed in Table 3. Figure 11(right) shows a map of the particle density distribution at each detector position and (left) their lateral distribution. Since the core position is located almost at the center of the Akeno branch and its arrival direction is near vertical, the systematic error in the estimation of S(600) described in Section 2.5 is quite small. The determined S(600) at the zenith angle 23° of this event is 892 m^{-2}. To estimate its uncertainty, we simulated many Monte Carlo events using the assumed systematic and statistical errors described in section 2.5. The fluctuation of $S_{23}(600)$ for this event is shown in figure 12.

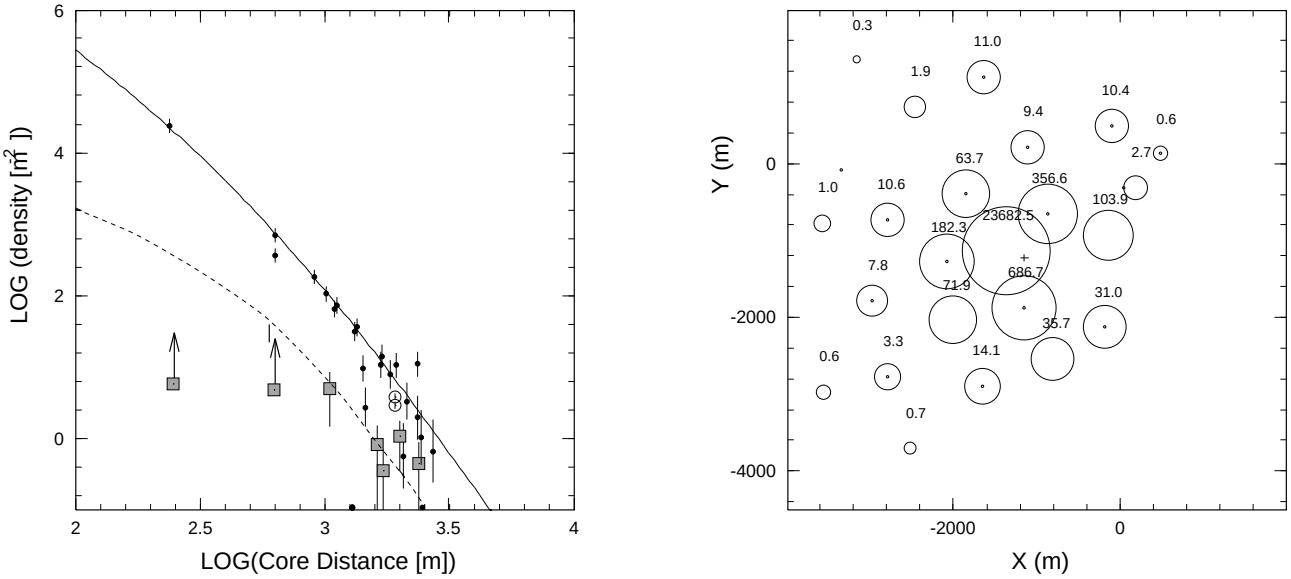

Figure 11: The highest energy event. Left: Lateral distribution of the charged particles (closed circles) and muons (shadowed squares). Open circles are densities obtained by the arrival time distribution of charged particles within 10μsec and 3.5μsec, respectively. The expected LDF and LDM extrapolated from the lower energy region are also shown by a solid and a dotted lines respectively. Right: The density map. A cross bar shows the estimated position of the shower core.

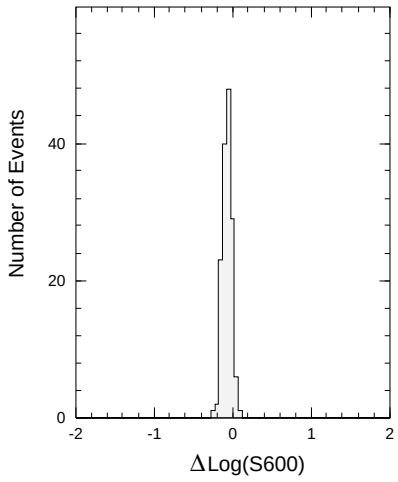

Figure 12: The fluctuation of S(600) determination for the highest energy event. This distribution has been obtained by the Monte Carlo simulation taking into account the fluctuations in the cascade development, detector resolution and the statistical errors.

The uncertainty in $S_{23}(600)$ is +21% and -6.6%. If we convert this density to the vertical $S_0(600)$ using the attenuation relation of Eq.(2) determined in the 10^{19}eV region, then $S_0(600) = 1065$ m^{-2}. If this shower is at maximum shower development, the observed $S_{23}(600)$ may not be attenuated and hence $S_0(600)$ is nearly equal to $S_{23}(600)$. Therefore $S_0(600)$ should be in the range $(892\sim1065)^{+21\%}_{-6.6\%} = (833\sim1289)$ m^{-2}.

The observed muon densities are also plotted in Figure 11. The lateral distribution function of muons for showers of energies between $10^{16.5}$ and $10^{19.5}$eV obtained by our recent analysis [19] is expressed by

$$\rho_\mu = N_\mu (C_\mu / R_0^2) r^{-0.75} (1+r)^{-2.52} \{(1+(R/800)^3\}^{-\delta} \qquad (12)$$

where $r = R/R_0$, $\delta \sim 0.6$, C_μ is the normalization constant, and N_μ is the total number of muons. The characteristic distance R_0 is given by

$$\log R_0 = 0.58(\sec\theta - 1) + 2.39. \qquad (13)$$

The muon LDF curve written in Figure 11(left) is the best fitted one to the data above 1000m from the core. The muon density at 600m from the core estimated from this curve is $42.8/\mathrm{m}^2$, which agrees well with $(30.9\pm9)/\mathrm{m}^2$ obtained by extrapolation from the lower energy region.

The distribution of arrival times of shower particles in this event was measured with scintillation detectors of $30\mathrm{m}^2$ area at 1920m from the core. The signal was recorded by a wave memory of 50nsec resolution [20]. The time spread of shower particles agrees with the expected spread based on extrapolation from lower energies.

These experiments may support validity of Eq.(1) up to $S(600)\sim10^3$. By extrapolating the S(600) vs energy relation given by Eq.(1) up to $S(600)\sim 10^3$, the energy of the present event is estimated to be $(1.7\sim2.6)\times10^{20}$eV. Details of this event are described in a separate paper [21].

4.DISCUSSION

4.1 Comparison with the Previous Akeno Result

The energy spectrum determined after correcting for the resolution of the AGASA array is expressed by Eq.(11) or Eq.(11′), depending on the ankle energy. These equations are in good agreement with that determined by the Akeno 1 km^2 array [10] in the overlapping energy region. The difference is only 5% in energy and is within the ambiguity of energy estimation errors of both experiments.

In figure 13, the present results are plotted by open circles after shifting experimental points in figure 10 to fit the most probable spectrum Eq.(11)

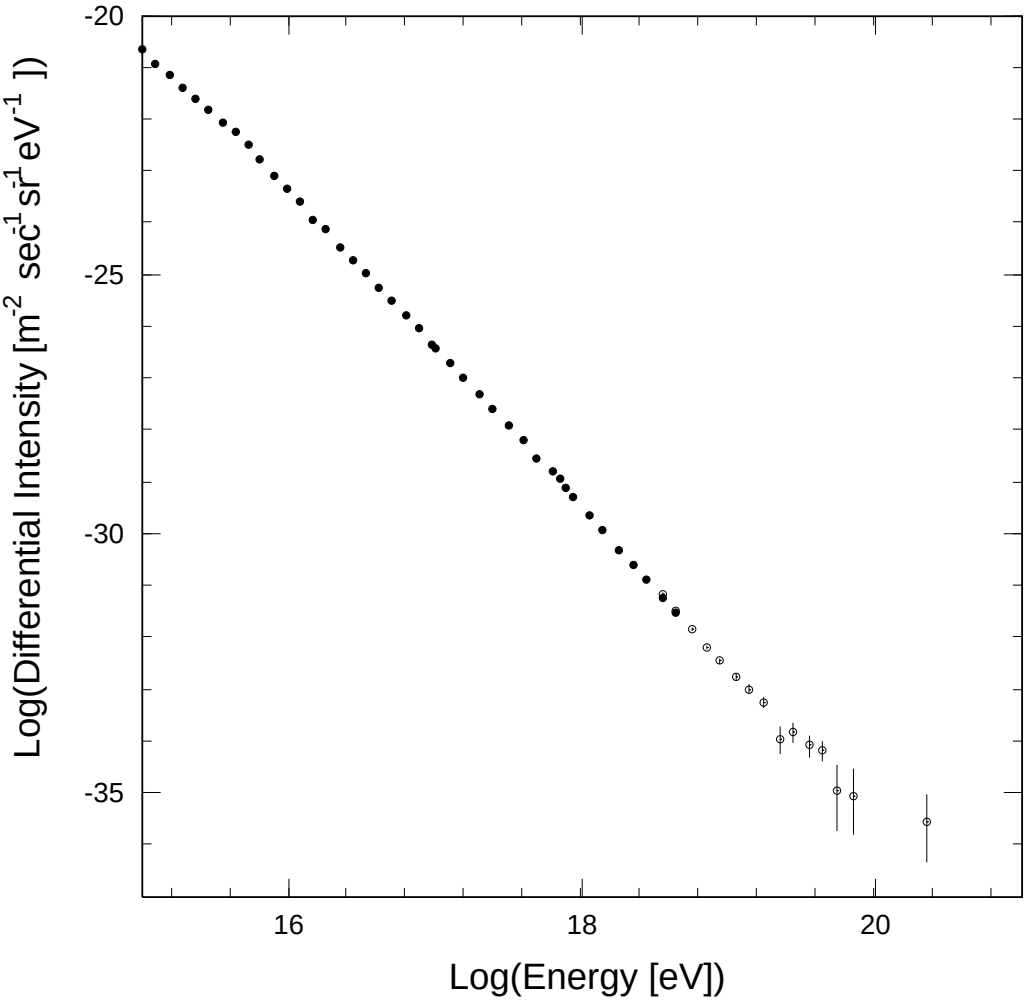

Figure 13: The energy spectrum of primary cosmic rays between $10^{14.5}$eV and $10^{20.5}$eV obtained at Akeno. Open circles are the present results by the AGASA by fitting the observed points to the Eq.(11) in $10^{18.5}$ $\sim 10^{19.0}$eV energy region.

Table 4: Comparison of various experiments on spectral slope in the flattening region and number of events observed and expected above 10^{20}eV.

Experiment	Slope	Ankle Energy eV	Number of Observed	Events $\geq 10^{20}$eV Expected
AGASA	$2.3^{+0.5}_{-0.3}$	10^{19}	1	5.2
	$2.7^{+0.2}_{-0.4}$	$10^{18.8}$	1	2.8
Fly's Eye (stereo)	2.71 ± 0.10	$10^{18.5}$	0	*0.8
(mono)			1	5.4
Haverah Park	$2.70^{+0.18}_{-0.17}$	10^{19}	4	3.2
Yakutsk	2.65 ± 0.10	$10^{18.85}$	1	8

* private communication from Dai.

or Eq.(11′) drawn by a solid line between $10^{18.5}$ and $10^{19.0}$eV. The closed circles are values from previous results determined with the *1km^2 array* [10]. This energy spectrum is the result of the Akeno experiment up to February 1994 between $10^{14.5}$ and 10^{20}eV.

4.2 Comparison with Other Experiments

The AGASA spectrum shown in figure 13 and the recent results of the Fly's Eye [9], the Haverah Park [8] and the Yakutsk [22] groups show general similarities in the spectral shape, although there are disagreements in the intensity and the energy of the ankle. These discrepancies can result from differences in energy resolution and systematic errors in primary energy estimation among the different experiments. Considering the differences in detection methods and energy estimation methods, the spectral discrepancies are rather small.

Table 4 lists the spectral slope in the flattening region, ankle energy and the number of events above 10^{20} eV observed and expected for each experiment. The flattening above around 10^{19}eV can be seen in each experiment and the slopes above ankle energy are about 2.7, in good agreement with each other. For AGASA, however, it should be noted that a flat slope such as 2.3 can also be accepted with a similar significance if we move the ankle energy. The situation is similar for the other experiments, so the ankle energy and the slope above the ankle energy are considered to be uncertain in each experiment.

The cutoff above 10^{20} eV seems to have been observed in the Fly's Eye and Yakutsk experiments, but not in the Haverah Park one. Our result favors the existence of a cutoff, but is not statistically significant. If we combine all the data observed in different groups without any energy renormalization, the number of events observed is 7 while 22 events would be

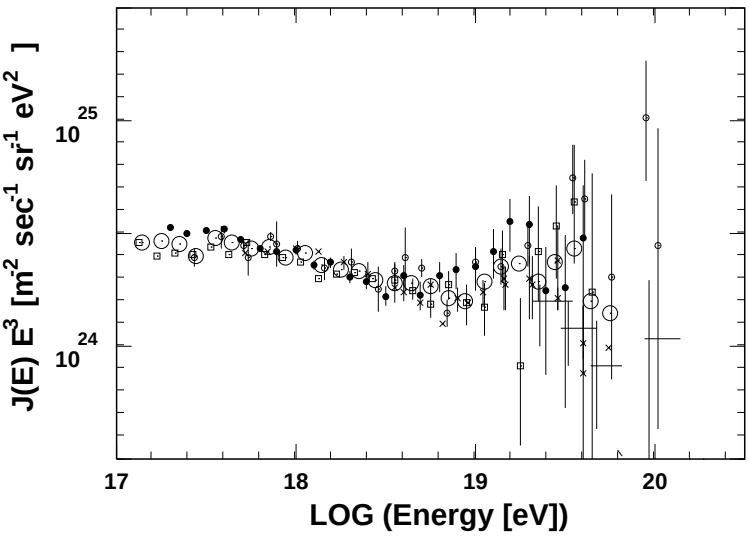

Figure 14: Folded energy spectra from the Haverah Park, the Yakutsk, the stereo Fly's Eye and the present results. All spectra are normalized to the stereo Fly's Eye result at around 10^{18}eV.

expected, and hence the evidence for a cutoff seems to be quite significant.

In figure 14, energy spectra are plotted after normalizing the Haverah Park, the Yakutsk and the present observed spectrum to the stereo Fly's Eye. Multiplication factors for energy in each experiment are 0.9, 0.8 and 0.8, respectively. Since the exposures of four experiments are rather similar, geometrical averages of the four experiments are calculated in each bin and plotted by large open circles in the same figure. It is found that spectral shape of all experiments agree with each other within 30% in energy and the ankle is clearly observed around $10^{18.9}$eV. A cutoff in the energy spectrum is also observed around $10^{19.6}$eV.

It would be more conclusive, if the cutoff could be determined with one experiment. We used in this analysis only showers whose cores hit well inside the boundary of each branch. There are about the same number of showers which hit between the branches, and hence we shall be able to determine the spectrum corresponding to the large open circles by our experiment alone with data up to the end of 1995.

4.3 Possible Models of Source Location

The present observation suggests the flattening of the spectrum slope around 10^{19} eV and a possible cut-off below 10^{20} eV. These features are expected from an extragalactic origin for the bulk of cosmic rays above

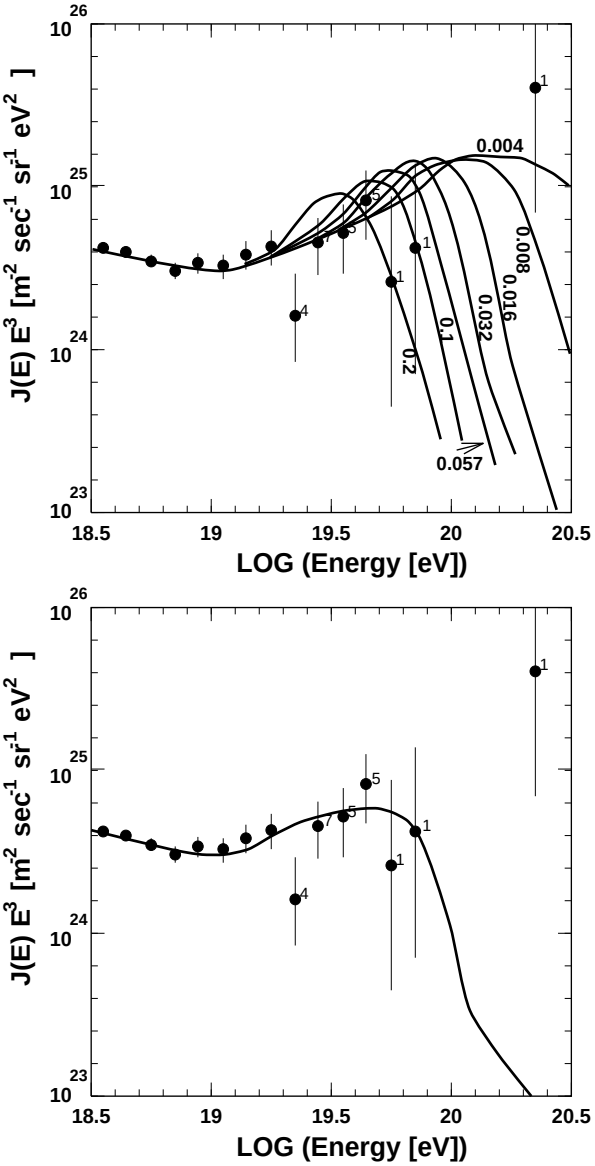

Figure 15: Spectra observed and expected for several models of source location. The curves are from the spectra obtained by Yoshida & Teshima (1993) [6] by taking the AGASA energy resolution into account. Top: A model in which all sources at the same redshift. Redshifts of the sources are shown beside the curves. Bottom: Diffuse Sources distributed isotropically in the Universe.

10^{19} eV. The flattening could result from dominance of the extragalactic cosmic rays over galactic ones and the spectrum cut-off might be the Greisen-Zatsepin-Kuźmin cutoff (GZK cutoff) due to the energy loss in the 2.7K photon field. We compare the present results with the expected spectra from models of source locations taking into account the AGASA energy resolution. The expected spectra are based on the calculation of the earlier paper [6], and an extragalactic component with an injection spectrum power index of -2.3 is assumed to dominate the galactic component above 10^{19} eV. Figure 15 compares the spectrum with expected spectra for extragalactic origin models, a single source at different distances (redshift z) and also the case of many sources distributed uniformly in the universe.

A model of many sources distributed uniformly in the Universe is in good agreement with the present experiment. For the case of a single source, the present result is best fitted to a source at redshift of larger than ~ 0.1 (450Mpc if the Hubble constant is 75km s^{-1} Mpc^{-1}). If nearby sources in the Virgo Cluster of galaxies (redshift 4×10^{-3} or 18Mpc -) or other clusters are responsible for the bulk of the highest energy cosmic rays and their energy spectrum extends much beyond 10^{20} eV, 5.6 events with energies above $10^{19.9}$ eV are expected to be observed, while no event has been observed except for the largest energy event whose arrival direction is quite different from the Virgo Cluster of galaxies.

The observed $(1.7\sim2.6)\times10^{20}$eV event seems inconsistent with the model described above because energy loss in intergalactic space should suppress such a high energy particles. A factor of three energy gap between the highest and the second highest energy event (6.7×10^{19} eV) suggests a quite different origin of the superhigh energy event from those below 10^{20}eV. The Fly's Eye group also observed a superhigh energy event with 3×10^{20} eV and there is more than a half-decade energy gap between the highest and the second highest event [9]. These superhigh energy events well beyond 10^{20} eV should stimulate the construction of the new generation of experiments with exposure more than an order of magnitude larger than those in operation.

5.SUMMARY

The cosmic ray energy spectrum above 3×10^{18} eV is determined. The flattening of the spectrum around 10^{19}eV (ankle) is observed with a significance of 2.9σ. If we express the differential energy spectrum of cosmic rays of energy E (in eV) with an ankle energy E_a as $J(E) = \kappa(E/E_a)^{-\gamma} m^{-2}\,\mathrm{sec}^{-1}\,sr^{-1}\mathrm{eV}^{-1}$, γ for $3\times\ 10^{18}\mathrm{eV} \leq E \leq E_a$ is in good agreement with the previous value 3.2 ± 0.1. The slope γ above E_a depends strongly on the value E_a. In the case E_a=10^{19}eV, $\kappa = (2.3^{+0.1}_{-0.2}) \times 10^{-33}$ and γ=$2.3^{+0.5}_{-0.3}$ for $10^{19}\mathrm{eV} \leq E \leq 10^{20}\mathrm{eV}$,

whereas in the case E_a=$10^{18.8}$eV, $\kappa = (1.0 \pm 0.1) \times 10^{-32}$ and γ=$2.7^{+0.2}_{-0.4}$ for $10^{18.8}$eV $\leq E \leq 10^{20}$eV. These spectra are determined after correcting for statistical errors and the energy resolution of the present experiment.

The number of events above $10^{19.9}$ eV expected from extrapolating the estimated primary spectrum beyond 10^{20} eV is 3$\sim$7 while one event has been observed with energy of $(1.7\sim2.6)\times10^{20}$eV. Assuming an extragalactic origin for cosmic rays above 10^{19}eV, localized sources at the redshift of greater than ~ 0.1 or many sources distributed uniformly in the Universe are acceptable within the scope of models considered. These possibilities will be discussed in another paper in relation to their arrival direction distribution. The existence of the $(1.7\sim2.6)\times10^{20}$eV particle suggests an origin at a nearby source, but its interpretation requires additional events.

ACKNOWLEDGEMENT

We are grateful to Akeno-mura, Nirasaki-shi, Sudama-cho, Nagasaka-cho, Takane-cho and Ohoizumi-mura for their kind cooperation. The authors also wish to acknowledge the valuable help by other members of the Akeno Group in the construction and maintenance of the array. We thank Dr. Paul Sommers of University of Utah for his careful reading of the manuscript and many valuable suggestions and Prof. A.A.Watson of University of Leeds for his valuable advices.

Appendix A. The Spectrum Monte Carlo

In order to derive the expected number of events in each energy bin for a given primary energy spectrum, we used the Monte Carlo simulation named the "spectrum Monte Carlo" taking into account both statistical fluctuation and energy determination error. The procedures in the simulation are the followings: For a given primary energy spectrum, dJ/dE, the expected total number of events above E_i is calculated by

$$N_{exp} = \ln 10 \int_{\log E_i}^{\infty} \frac{dJ}{dE} A(\log E) E d(\log E), \qquad (A-1)$$

where $A(\log E)$ is the exposure of the array as a function of primary energy. We then decide the total number of events N_{tot} for a particular run by sampling from the Gaussian distribution with an mean value N_{exp}. For each event of N_{tot}, the primary energy is assigned in sequence by sampling the probability distribution, where the proportion of having its energy below E is given by

$$R(E) = \frac{\ln 10}{N_{exp}} \int_{\log E_i}^{\log E} \frac{dJ}{dE} A(\log E) E d(\log E). \qquad (A-2)$$

Then the zenith angle of each event is assinged by sampling in the similar zenith angle distribution of the observed data. Assigned zenith angle and primary energy give $\mathrm{S}_\theta(600)$ for each event. The $\mathrm{S}_\theta(600)$ corresponding to the expected one for an assigned θ and E is determined by sampling from the fluctuation distribution as shown in Figure 6 which includes the determination error. After assigning $\mathrm{S}_\theta(600)$ to total N_{tot} events and converting them to energy by Eq.(1) and Eq.(2), the energy spectrum for one run with the same exposure as in the experiment is determined. Many trials of these procedures give the most probable number of events for a given primary energy spectrum. We have confirmed that the distribution of number of events in each energy bin is expressed in conformity to the Poissonian.

REFERENCES

1. K. Greisen, Phys.Rev.Lett. **16** (1966) 748
2. G.T.Zatsepin and V.A.Kuźmin, Pisma Zh.Eksp.Teor.Fiz. **4** (1966) 114.
3. J.L.Puget, F.W.Stecker and J.H.Bredekamp, Ap.J. **205** (1976) 638.
4. C.T.Hill and D.N.Schramm, Phys.Rev.D **31** (1985) 564.
5. V.S.Berezinsky and S.I. Grigor'eva , Astron. Astrophys. **199** (1988) 1.
6. S.Yoshida and M.Teshima, Prog.Theor.Phys. **89** (1993) 833.
7. J.Linsley, J. Phys. G: Nucl. Phys., **12** 51 (1986).
8. M.A.Lawrence, R.J.O.Reid and A.A.Watson *J.Phys.G:Nucl.Phys.* **17** (1991) 733.
9. D.J.Bird, S.C.Corbato, H.Y.Dai, B.R.Dawson, J.W.Elbert, B.L.Emerson, K.D.Green, M.A.Huang, D.B.Kieda, M.Luo, S.Ko, C.G.Larsen, E.C.Loh, M.H.Salamon, J.D.Smith, P.Sokolsky, P.Sommers, J.K.K.Tang and S.B.Thomas, Ap.J. **424** (1994) 491.
10. M.Nagano, M.Teshima, Y.Matsubara, H.Y.Dai, T.Hara, N.Hayashida, M.Honda, H.Ohoka and S.Yoshida, J.Phys.G: Nucl.Part.Phys. **18** (1992) 423.
11. N.Chiba, K.Hashimoto, N.Hayashida, K.Honda, M.Honda, N.Inoue, F.Kakimoto, K.Kamata, S.Kawaguchi, N.Kawasumi, Y.Matsubara, K.Murakami, M.Nagano, S.Ogio, H.Ohoka, To.Saito, Y.Sakuma, M.Teshima, I.Tsushima, T.Umezawa, S.Yoshida and H.Yoshii, Nucl. Instrum. Methods **A311** (1992) 338.
12. M.M.Winn, J.Ulrichs, L.S.Peak, C.B.A.McCusker and L.Horton, J.Phys.G: Nucl. Phys. **12** (1986) 653.
13. N.N.Efimov, N.N.Efremov, A.V.Glushkov, I.T.Makarov, P.D.Petrov and M.I.Pravdin, Proc. 22nd ICRC, Dublin 4 (1991) 339.
14. A.M.Hillas, D.J.Marsden, J.D.Hollows and H.W.Hunter, Proc.12th ICRC, Hobart **3**, (1971) 1001.
15. H.Y.Dai, K.Kasahara, Y.Matsubara, M.Nagano and M.Teshima, J.Phys.G: Nucl.Phys. **14** (1988) 793.

16. S.Yoshida, N.Hayashida, K.Honda, M.Honda, S.Imaizumi,N.Inoue, K.Kadota, F.Kakimoto, K.Kamata, S.Kawaguchi, N.Kawasumi, Y.Matsubara, K.Murakami, M.Nagano, H.Ohoka, Y.Suzuki, M.Teshima, I.Tsushima and H.Yoshii, J.Phys.G : Nucl.Part.Phys. **20** (1994) 651.

17. T.Hara, Y.Hatano, N.Hayashida, F.Ishikawa, N.Jogo, K.Kamata, T.Kifune, M.Nagano, Y.Ohno, H.Ohoka, R.Torii, G.Tanahashi, M.F.Crouch, S.Kawaguchi, N.Nii, M.Machida, T.Matano, K.Ohta, H.Sakuyama, K.Jitsuno, K.Hashimoto, K.Honda, N.Kawasumi, I.Tsushima, F.Arimura, N.Awaji, Y.Hayashi, N.Ito, S.Kawakami, N.Hasebe and H.Yoshii, Proc.16th ICRC, Kyoto **8** (1979) 135.

18. M.Teshima, Y.Matsubara, T.Hara, N.Hayashida, M.Honda, F.Ishikawa, K.Kamata, T.Kifune, M.Mori, M.Nagano, K.Nishijima, H.Ohoka, Y.Ohno and G.Tanahashi, J.Phys.G: Nucl.Phys. **12** (1986) 1097.

19. N.Chiba, N.Hayashida, K.Honda, M.Honda, S.Imaizumi,N.Inoue, K.Kadota, F.Kakimoto, K.Kamata, S.Kawaguchi, N.Kawasumi, Y.Matsubara, K.Murakami, M.Nagano, H.Ohoka, Y.Suzuki, M.Teshima, I.Tsushima, S.Yoshida and H.Yoshii, Proc. 23rd ICRC, Calgary **4** (1993) 307.

20. K.Honda, K.Hashimoto, N.Kawasumi, I.Tsushima, N.Inoue and T.Matano, Proc. 23rd ICRC, Calgary, **4** 311 , (1993)

21. N.Hayashida, K.Honda, M.Honda, S.Imaizumi, N.Inoue, K.Kadota, F.Kakimoto, K.Kamata, S.Kawaguchi, N.Kawasumi, Y.Matsubara, K.Murakami, M.Nagano, H.Ohoka, M.Takeda, M.Teshima, I.Tsushima, S.Yoshida, and H.Yoshii, ICRR-Report-324-94-19 (1994) (Institute for Cosmic Ray Research, University of Tokyo)

22. B.N.Afanasiev, M.N.Dyakonov, T.A.Egorov, V.P.Egorova, A.N.Efimov, N.N.Efremov, A.V.Glushkov, S.P.Knurenko, V.A.Kolosov, A.D.Krasilinikov, I.T.Makarov, A.A.Mikhailov, E.S.Nikiforova, V.A.Orlov, M.I.Pravdin, I.Ye.Sleptsov, N.I.Sleptsov, G.G.Struchkov, in: Proc. Tokyo Workshop on Techniques for the Study of the Extremely High Energy Cosmic Rays, eds M.Nagano and M.Teshima (Institute for Cosmic Ray Research, Univ. of Tokyo 1993) p.35